AIAA SciTech Forum
11–15 & 19–21 January 2021, VIRTUAL EVENT
AIAA Scitech 2021 Forum

10.2514/6.2021-1237

Derivative-Free Line-Search Algorithm for Multi-Fidelity Optimization

Giampaolo Liuzzi *
CNR-IASI, National Research Council-Institute for System Analysis and Computer Science, Rome, Italy

Stefano Lucidi †
Sapienza University, Rome, Italy

Francesco Rinaldi ‡
University of Padua, Padua, Italy

Riccardo Pellegrini §, Andrea Serani ¶, and Matteo Diez ‖
CNR-INM, National Research Council-Institute of Marine Engineering, Rome, Italy

The paper presents a multi-fidelity coordinate-search derivative-free algorithm for non-smooth constrained optimization (MF-CS-DFN), in the context of simulation-based design optimization (SBDO). The objective of the work is the development of an optimization algorithm able to improve the convergence speed of the SBDO process. The proposed algorithm is of a line-search type and can handle objective function evaluations performed with variable accuracy. The algorithm automatically selects the accuracy of the objective function evaluation based an internal steplength parameter. The MF-CS-DFN algorithm starts the optimization with low accuracy and low-cost evaluations of the objective function, then the accuracy (and evaluation cost) is increased. The method is coupled with a potential flow solver whose accuracy is determined by the computational grid size. No surrogate models are used in the current study. The algorithm is applied to the hull-form optimization of a destroyer-type vessel in calm water using 14 hull-shape parameters as design variables. The optimization aims at the total resistance reduction. Seven refinements of the computational grid are used by the multi-fidelity optimizations. Four setups of the MF-CS-DFN algorithm are tested and compared with an optimization performed only on the finest grid. The results show that three of the tested setups achieve better performance than the high-fidelity optimization, converging to a lower resistance value with a reduced computational cost.

I. Introduction

The definition of new improved designs of aerial, ground, or marine vehicles is of upmost importance. This because there exists the urgency of significantly reducing the pollutant emission. Furthermore, there is the needing of improving the safety in environments where the operating conditions (such as the sea state) are subject to a significant uncertainty and may turn extreme. Finally, new designs are necessary to meet the technological evolution in transportation (such as hydrogen or battery powered vehicles).

From an engineering viewpoint, the simulation-based design optimization (SBDO) procedure has proven its ability to help designers in achieving optimal design solutions. SBDO procedure combines (i) design modification, (ii) numerical solvers, and (iii) optimization algorithms. The use of optimization algorithms usually requires a large number of function evaluations to converge to the optimal solution. This can make the SBDO procedure very expensive from a computational viewpoint, when high-fidelity solvers are used to compute the desired outputs. For this reason, to reduce the computational burden of SBDO, multi-fidelity (MF) methods [1] can be used to combine the accuracy of high-fidelity solvers with the computational cost of low-fidelity solvers.

*Research Scientist, CNR-IASI, Via dei Taurini, 19, 00185
†Full Professor, Department of Computer, Control, and Management Engineering "A. Ruberti", Via Ariosto, 25, 00185
‡Associate Professor, Department of Mathematics, Via Trieste, 63, 35131
§Postdoctoral Research Fellow, CNR-INM, Via di Vallerano 139, 00128, AIAA Member, riccardo.pellegrini@inm.cnr.it
¶Research Scientist, CNR-INM, Via di Vallerano 139, 00128
‖Senior Research Scientist, CNR-INM, Via di Vallerano 139, 00128, AIAA Member, matteo.diez@cnr.it

Usually, multi-fidelity methods take advantage of surrogate models to perform a data fusion of the available fidelities within a single multi-fidelity surrogate model (*e.g.*, co-kriging [2]), or to correct low-fidelity trained surrogate models with the surrogate models of the errors between fidelities [3]. Examples of multi-fidelity surrogate models are reported for non-intrusive polynomial chaos [4], Gaussian Process [5], and radial basis functions [6].

Here is proposed an example of a deterministic derivative-free line-search type algorithms that make use of objective function evaluations with variable fidelity, without the interposition of a surrogate model.

The objective of the present work is the development of a derivative-free line-search type algorithm [7] able to use objective function evaluations with different levels of accuracy. The latter can be provided by *e.g.* using different physical models (potential flow, Reynolds-averaged Navier-Stokes equations, etc.) or varying the numerical accuracy (grid refinement, time step, etc.) of the numerical solver within the same physical model. The algorithm automatically selects the fidelity used for the objective function evaluation: starting from the lowest fidelity, it moves to higher fidelities as it converges towards the minimum. Derivative-free algorithms are preferred since the numerical evaluation of the objective function may be affected by unavoidable numerical noise. Such noise may negatively affect the convergence of derivative-based algorithms, if derivatives are not directly provided (*e.g.*, adjoint solvers).

Beran et al. [1] have proposed a classification of benchmark problems for variable-fidelity methods. The classification is based on the complexity of the benchmark, from the most simple (L1) to the most complex (L3). In this work the method is demonstrated for an L2 problem. The quantity of interest is computed from the solution of partial differential equations with a moderate computational cost and some engineering idealizations are made to simplify the problem. Specifically, the application pertains to the hull-form optimization of the DTMB 5415 model, an open-to-public model of a naval destroyer. Ship performance is evaluated by a potential flow solver (WARP [8], developed at CNR-INM) and a simplified hull geometry is used (with no propellers, appendages, etc.). The objective function evaluations are not used to train a surrogate model, therefore the proposed algorithm performs a new simulation for each objective function evaluation. The optimization aims to minimize the total resistance in calm water at even keel. The multi-fidelity is provided by using seven grids with constant refinement. Grid-size convergence and grid error (E_G) are assessed and discussed. The hull-shape is modified by using 14 design variables. Four setups of the proposed MF-CS-DFN algorithm are compared with an optimization performed only with the finest grid.

II. Multi-Fidelity Linesearch-Based Derivative-Free Approach for Nonsmooth Constrained Optimization Algorithm

Considering the bound-constrained and single-objective minimization problem

$$\begin{aligned} &\text{minimize} && f(\mathbf{x}) \\ &\text{subject to} && \mathbf{x} \in X, \end{aligned} \tag{1}$$

where X is the set of bound constraints on the variables, i.e.,

$$X = \{\mathbf{x} \in \mathbb{R}^N : \mathbf{x}_l \leq \mathbf{x} \leq \mathbf{x}_u\}, \tag{2}$$

and f is Lipschitz continuous. Since the domain lower ($\mathbf{x}_l$) and upper ($\mathbf{x}_u$) boundaries are both finite, the set X is compact. In the following, an extension of the linesearch-based derivative-free approach for nonsmooth constrained optimization (CS-DFN) [7] is proposed for the solution of the aforementioned problem with a multi-fidelity approach. Specifically, a multi-fidelity (MF) variant of CS-DFN is developed (MF-CS-DFN), able to manage evaluations of the objective function performed with variable accuracy, see Algorithm 1.

The proposed algorithm first explores the i-th coordinate direction $\mathbf{e}^i$ with a tentative steplength $\tilde{\alpha}^i$, evaluating the objective function with the lowest accuracy. The Continuous Search procedure [9, 10] is used to identify a steplength α^i that can guarantee a sufficient reduction of the objective function along the $\mathbf{e}^i$ direction, see Algorithm 2. The Continuous Search procedure takes in input the tentative steplength $\tilde{\alpha}^i$, the current point $\mathbf{y}$ and a direction $\mathbf{p}$ and returns in output the actual step α and the computed direction $\mathbf{p}_{new}$ which is equal to $\pm\mathbf{p}$. The procedure explores a direction $\mathbf{p}$ searching for the largest nonnegative integer j such that sufficient decrease is obtained at point $\mathbf{y} + \delta^{-j}\tilde{\alpha}\mathbf{p}$, $\delta \in (0, 1)$. If direction $\mathbf{p}$ cannot provide sufficient decrease, then the opposite direction is tested before declaring a failure, thus returning the null step $\alpha = 0$. When the null stepsize is returned after exploration of direction $\tilde{\alpha}^i$, the method decreases the tentative step for next iteration, i.e. $\tilde{\alpha}^i_{new} = \theta\tilde{\alpha}_i$, $\theta \in (0, 1)$. Otherwise, the tentative step for the next iteration is possibly augmented by setting $\tilde{\alpha}^i_{new} = \alpha$.

Algorithm 1 MF-CS-DFN

Input. $\theta \in (0,1)$, $\eta > 0$, $\mathbf{x}_0 \in X$, $\tilde{\alpha} > 0$, $\tilde{\alpha}^i > 0$, $\mathbf{d}^i = \mathbf{e}^i$, for i=1, ..., N such that $||\mathbf{d}^i|| = 1$
Let $\pi_1, \ldots, \pi_r$ with $r \geq 1$ be the precision levels, such that $\pi_i + 1 < \pi_i$, $i = 1, \ldots, r-1$
Set $\bar{\jmath} \leftarrow 1$ and $\mathbf{x} \leftarrow \mathbf{x}_0$

for $k = 0, 1, \ldots$ **do** ▷ Start the iterations
  Set $\mathbf{y} \leftarrow \mathbf{x}$
  for $i = 1, \ldots, N$ **do**
    Compute α and $\mathbf{d}^i_{new}$ by the *Continuous Search* $(\tilde{\alpha}^i, \mathbf{y}, \mathbf{d}^i; \alpha, \mathbf{d}^i_{new})$ ▷ Call the continuous search
    if $(\alpha = 0)$ **then**
      Set $\tilde{\alpha}^i_{new} = \theta\tilde{\alpha}^i$
    else
      Set $\tilde{\alpha}^i_{new} = \alpha$
    Set $\alpha^i \leftarrow \alpha$, $\mathbf{d}^i \leftarrow \mathbf{d}^i_{new}$, $\mathbf{y} \leftarrow \mathbf{y} + \alpha\mathbf{d}^i_{new}$
  if $(\max_{i=1,\ldots,n}\{\alpha^i, \tilde{\alpha}^i\} \leq \eta)$ **then**
    Compute α and $\tilde{\mathbf{d}}$ by the *Projected Continuous Search* $(\tilde{\alpha}, \mathbf{y}, \mathbf{d}_k; \alpha, \tilde{\mathbf{d}})$ ▷ Call the projected continuous search
    if $(\alpha = 0)$ **then**
      $\tilde{\alpha}_{new} = \theta\tilde{\alpha}$
    else
      $\tilde{\alpha}_{new} = \alpha$ and $\mathbf{y} \leftarrow [\mathbf{y} + \alpha\tilde{\mathbf{d}}]_{[\mathbf{x}_l, \mathbf{x}_u]}$
  else
    Set $\tilde{\alpha}_{new} = \tilde{\alpha}$
  if $(\max_{i=1,\ldots,n}\{\alpha^i, \tilde{\alpha}^i\} \leq \pi_{\bar{\jmath}}$ **and** $\bar{\jmath} < r)$ **then**
    $\bar{\jmath} \leftarrow \bar{\jmath} + 1$ ▷ Increase the accuracy
  Set $\tilde{\alpha} \leftarrow \tilde{\alpha}_{new}$, $\tilde{\alpha}^i \leftarrow \tilde{\alpha}^i_{new}$, for $i = 1, \ldots, N$
  Find $\mathbf{x} \in X$ such that $f_{\pi_{\bar{\jmath}}}(\mathbf{x}) \leq f_{\pi_{\bar{\jmath}}}(\mathbf{y})$

Algorithm 2 Continuous Search $(\tilde{\alpha}, \mathbf{y}, \mathbf{p}; \alpha, \mathbf{p}^+)$

Data. $\gamma > 0$, $\delta \in (0,1)$
Step 1. Compute the largest $\bar{\alpha}$ such that $\mathbf{y} + \bar{\alpha}\mathbf{p} \in X$. Set $\alpha = \min\{\bar{\alpha}, \tilde{\alpha}\}$
Step 2. If $\alpha > 0$ and $f_{\pi_{\bar{\jmath}}}(\mathbf{y} + \alpha\mathbf{p}) \leq f_{\pi_{\bar{\jmath}}}(\mathbf{y}) - \gamma\alpha^2$ **then** set $\mathbf{p}_{out} = \mathbf{p}$ and go to Step 6
Step 3. Compute the largest $\bar{\alpha}$ such that $\mathbf{y} - \bar{\alpha}\mathbf{p} \in X$. Set $\alpha = \min\{\bar{\alpha}, \tilde{\alpha}\}$
Step 4. If $\alpha > 0$ and $f_{\pi_{\bar{\jmath}}}(\mathbf{y} - \alpha\mathbf{p}) \leq f_{\pi_{\bar{\jmath}}}(\mathbf{y}) - \gamma\alpha^2$ **then** set $\mathbf{p}_{out} = -\mathbf{p}$ and go to Step 6
Step 5. Set $\alpha = 0$, **return** α and $\mathbf{p}_{out} = \mathbf{p}$
Step 6. Let $\beta = \min\{\bar{\alpha}, (\alpha/\delta)\}$
Step 7. If $\alpha = \bar{\alpha}$ or $f_{\pi_{\bar{\jmath}}}(\mathbf{y} + \beta\mathbf{p}_{out}) > f_{\pi_{\bar{\jmath}}}(\mathbf{y}) - \gamma\beta^2$ **return** α and $\mathbf{p}_{out}$
Step 8. Set $\alpha = \beta$ and go to Step 6

Provided that the actual (α^i) and tentative ($\tilde{\alpha}^i$) steplengths are smaller than a given threshold $\eta > 0$, a further direction $\mathbf{d}$ is explored through the Projected Continuous Search procedure, see Algorithm 3. This procedure carries out an exploration along direction $\mathbf{p}$ (or $-\mathbf{p}$ if needed). However, since the direction $\mathbf{p} = \mathbf{d}$ used by the Projected Continuous Search is not equal to $\pm\mathbf{e}^i$ for some $i \in \{1, \ldots, N\}$, projections onto X must be taken to ensure feasibility of the generated points. Then, given the current point $\mathbf{y}$ at step k, the procedure first evaluates the function at $[\mathbf{y} \pm \tilde{\alpha}\mathbf{d}_k]_{[\mathbf{x}_l, \mathbf{x}_u]}$. In case a sufficient reduction of the function value is obtained, then an extrapolation along the search direction is performed, so that a suitable step-length α is computed, and is used as a tentative steplength for the next iteration, i.e., $\tilde{\alpha}_{new} = \alpha$. On the other hand, if at $[\mathbf{y} \pm \tilde{\alpha}\mathbf{d}_k]_{[\mathbf{x}_l, \mathbf{x}_u]}$ a sufficient reduction of the function value is not obtained, then the tentative steplength at the next iteration is suitably reduced by a scale factor, i.e., $\tilde{\alpha}_{new} = \theta\tilde{\alpha}$, $\theta \in (0,1)$.

If the steplengths in all directions are all below η and the accuracy used to evaluate the objective function is not the highest, the accuracy is increased and the steplengths are reinitialized. The process is repeated until the convergence of the algorithm is achieved with the highest accuracy available.

Algorithm 3 Projected Continuous Search $(\tilde{\alpha}, \mathbf{y}, \mathbf{p}; \alpha, \mathbf{p}_{out})$

Data. $\gamma > 0$, $\delta \in (0, 1)$
Step 0. Set $\alpha = \tilde{\alpha}$
Step 1. **If** $f([\mathbf{y} + \alpha\mathbf{p}]_{[\mathbf{x}_l, \mathbf{x}_u]}) \leq f(\mathbf{y}) - \gamma\alpha^2$ **then** set $\mathbf{p}_{out} = \mathbf{p}$ and go to Step 4
Step 2. **If** $f([\mathbf{y} - \alpha\mathbf{p}]_{[\mathbf{x}_l, \mathbf{x}_u]}) \leq f(\mathbf{y}) - \gamma\alpha^2$ **then** set $\mathbf{p}_{out} = -\mathbf{p}$ and go to Step 4
Step 3. Set $\alpha = 0$, **return** α and $\mathbf{p}_{out} = \mathbf{p}$
Step 4. Let $\beta = \alpha/\delta$
Step 5. **If** $f([\mathbf{y} + \beta\mathbf{p}_{out}]_{[\mathbf{x}_l, \mathbf{x}_u]}) > f(\mathbf{y}) - \gamma\beta^2$ **return** $\alpha, \mathbf{p}_{out}$
Step 8. Set $\alpha = \beta$ and go to Step 4

III. L2 Application: DTMB 5415 Hull-Shape Optimization

The optimization aims to the total resistance (R) minimization in calm water at Fr = 0.28 of the DTMB 5415 model. Figure 1 shows the geometry of the CNR-INSEAN 2340 model, a geosym replica of the DTMB 5415 model used for towing tank experiments. The optimization problem can be written as

$$\begin{aligned} \text{minimize} \quad & R(\mathbf{x}), \qquad \text{with} \qquad \mathbf{x} \in \mathbb{R}^N \\ \text{subject to} \quad & L_{\text{pp}}(\mathbf{x}) = L_{\text{pp}_0}, \\ \text{and to} \quad & \nabla(\mathbf{x}) = \nabla_0, \\ & |\Delta B(\mathbf{x})| \leq 0.05 B_0, \\ & |\Delta T(\mathbf{x})| \leq 0.05 T_0, \\ & V(\mathbf{x}) \geq V_0, \\ & \mathbf{x}_l \leq \mathbf{x} \leq \mathbf{x}_u, \end{aligned} \tag{3}$$

where $\mathbf{x}$ are the design variables, $\mathbf{x}_l$ and $\mathbf{x}_u$ are the lower and upper boundaries, L_{pp} is the length between perpendiculars of the hull, B is the hull beam, T is the drought, and V is the volume reserved for the sonar in the dome, corresponding to 4.9 m diameter and 1.7 m length (cylinder). Subscript "0" indicates original-geometry values. Equality and inequality constraints on the geometry deformations are based on [11]. Table 1 summarizes the main characteristics of the hull and test conditions.

A. Hydrodynamic Solver

The WAve Resistance Program (WARP) code, developed by the CNR-INM [8], is used for the numerical solution of the potential flow equations. For the current application, wave resistance computations are based on the linear potential flow theory, with Dawson (or double-model) linearization. The wave resistance is evaluated using a pressure integral over the body surface, whereas the frictional resistance is estimated using a flat-plate approximation based on the local Reynolds number. In this work seven levels of fidelity are used, corresponding to seven grid sizes with a refinement ratio of $2^{0.25}$. Table 2 summarizes the grid size, nodes number (M), and the error (E_G) associated to each grid.

Figure 2 shows the convergence of the hull total resistance versus the grid refinement level. All the grids from G1 to G6 lies on the linear reference that is the theoretical convergence rate for this solver. The only outlier is the coarsest grid, the G7. This grid is still providing results that are physically acceptable, see Fig. 3g, but is clearly out of the convergence rate.

Table 1 DTMB 5415 original (model scale) hull main particulars.

Quantity	Symbol	Unit	Value
Displacement	∇	m^3	0.549
Length between perpendiculars	L_{pp}	m	5.720
Beam	B	m	0.760
Draft	T	m	0.248
Froude number	Fr	–	0.280

(a) A 5.720 m length model of the DTMB 5415 (CNR-INSEAN model 2340)

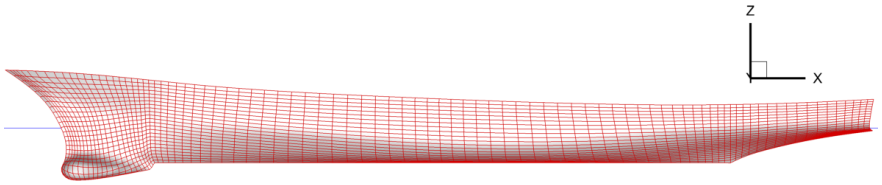

(b) Hull grid (G3)

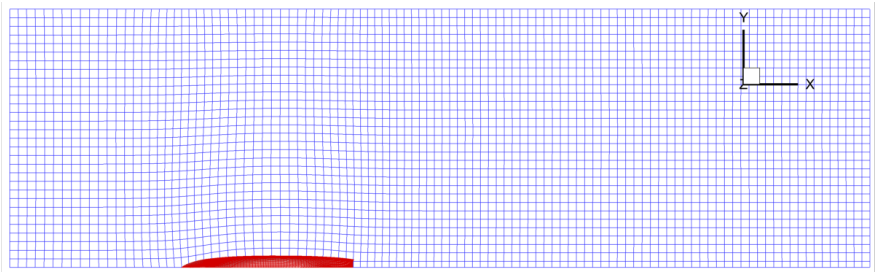

(c) Free-surface grid (G3)

Fig. 1 Hull and free-surface grids (G3).

The error E_G associated to each grid level is evaluated as the error between the computed resistance and the resistance of a reference solution, G0. The latter is identified along the linear regression (considering G1, G2, G3, and G4 only) of the resistance versus $1/\sqrt{M}$. G0 is extrapolated as the refinement of G1 with ratio $2^{0.25}$, see Fig. 2. The error is evaluated for the original hull and, for the sake of simplicity, it is considered constant within the design space.

Figure 3 shows the pressure contour on the hull and the wave elevation predicted for each grid. The finest grid (G1) predicts a higher pressure on the bow of the hull and higher wave elevation then the other grids.

Table 2 Potential flow solver grid details.

Refinement ratio	Grid level (G)	Hull nodes	Free-surface nodes	Total nodes (M)	Error (E_G) [%]
$2^{0.25}$	1	180×50	150×44	15.6k	1.2
	2	151×42	126×37	11.0k	2.0
	3	127×35	106×31	7.7k	3.0
	4	107×30	90×26	5.5k	5.3
	5	90×25	75×22	3.9k	7.4
	6	76×21	64×19	2.8k	9.5
	7	64×18	54×16	2.0k	18.9

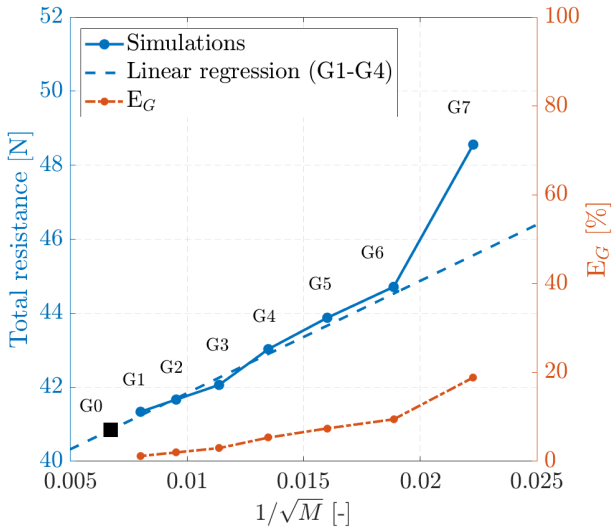

Fig. 2 Grid convergence of the potential flow solver.

B. Hull-Shape Modifications

The shape modifications $\tilde{\boldsymbol{\gamma}}(\boldsymbol{\xi}, \mathbf{x})$ are produced directly on the Cartesian coordinates $\boldsymbol{\xi}$ of the computational body surface grid $\mathbf{g}$, as per

$$\mathbf{g}(\boldsymbol{\xi}, \mathbf{x}) = \mathbf{g}_0(\boldsymbol{\xi}) + \boldsymbol{\gamma}(\boldsymbol{\xi}, \mathbf{x}) \tag{4}$$

where $\boldsymbol{\gamma}$ is a shape modification vector obtained by a physics-informed design-space dimensionality reduction [12, 13]

$$\boldsymbol{\gamma}(\boldsymbol{\xi}, \mathbf{x}) = \sum_{k=1}^{N} x_k \boldsymbol{\psi}_k(\boldsymbol{\xi}) \tag{5}$$

with $\boldsymbol{\psi}$ a set of orthonormal functions. The original design space is defined as linear superposition of orthogonal functions and has a dimension of 27 variables [11], whereas in this work $N = 14$ design variables ($\mathbf{x}$) are used. It is important to consider that the new variables defined by the dimensionality reduction procedure have a hierarchical order. This means that the first variables have a greater effect on the hull-shape modification than the last.

IV. Numerical Results

Four combinations of threshold η and $\tilde{\alpha}$ reinitialization values are tested. Specifically, two threshold values and two steplength reinitialization values are used as summarized in Tab. 3. Setups A use a static threshold value, with A1 using a static and A2 dynamic reinitialization of the steplength. Setups B use a dynamic threshold value, with B1 using a static and B2 dynamic reinitialization of the steplength.

The performance of the MF-CS-DFM algorithm is assessed comparing the convergence of the multi-fidelity (MF) optimizations with the convergence of a high-fidelity (HF) optimization (where the objective function is evaluated

Table 3 Steplength threshold and reinitialization values for each MF-CS-DFN setup.

Setup	η	$\tilde{\alpha}_{\pi_j}$ reinitialization value
A1	10^{-3}	1
A2	10^{-3}	$10\ \alpha_{\pi_{j+1}}$
B1	E_G	1
B2	E_G	$10\ \alpha_{\pi_{j+1}}$

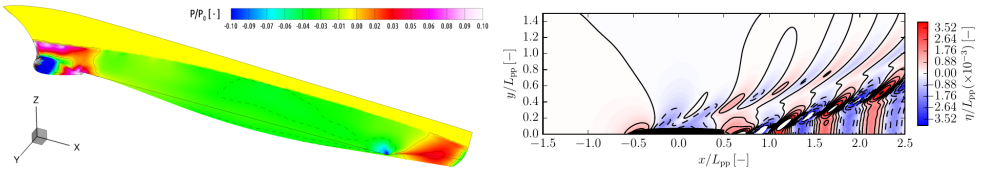

(a) G1

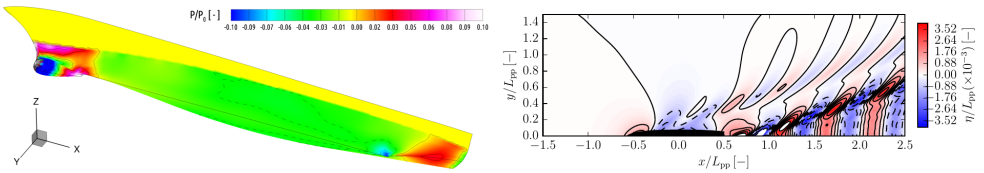

(b) G2

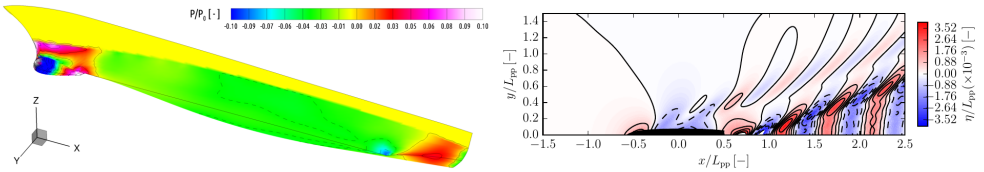

(c) G3

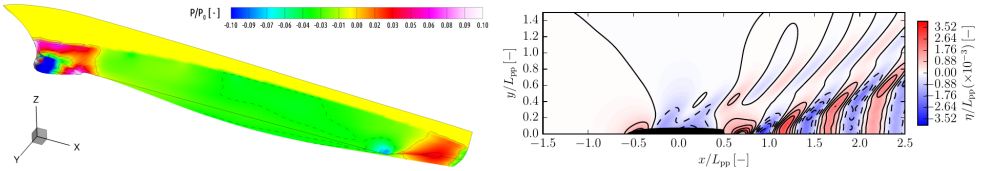

(d) G4

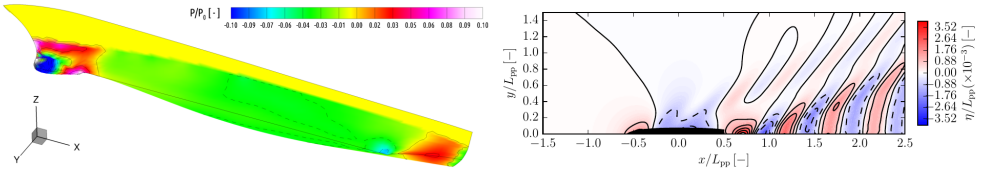

(e) G5

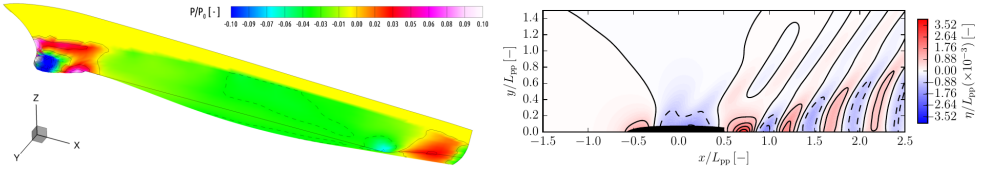

(f) G6

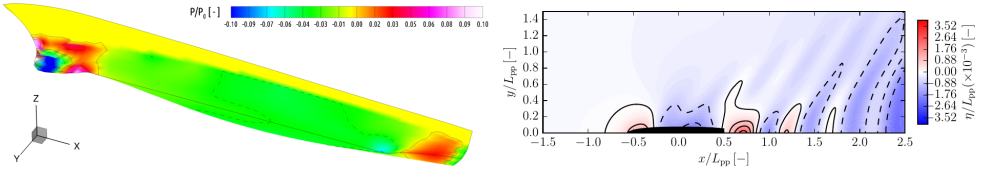

(g) G7

Fig. 3 Pressure on hull (left) and free-surface elevation (right) of the original hull varying the grid refinement.

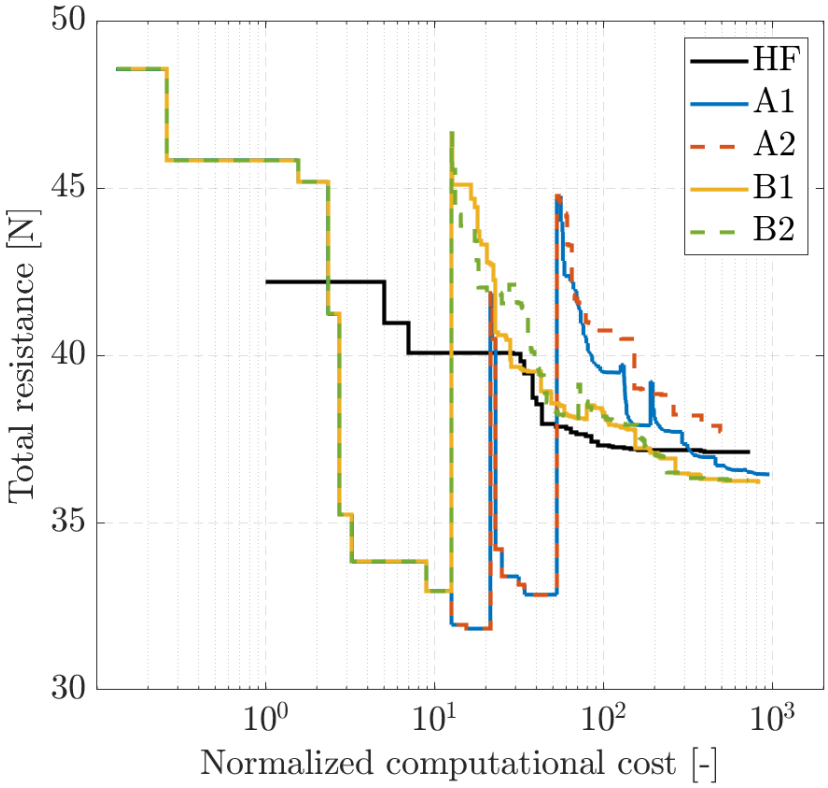

Fig. 4 Convergence of the total resistance.

only with high-fidelity simulations). A normalized computational cost is used for the convergence analysis, where an objective function evaluation on the finest grid is equal to one and the evaluations on the less refined grids are equal to $[0.70, 0.50, 0.35, 0.25, 0.18, 0.13]$ from G2 to G7.

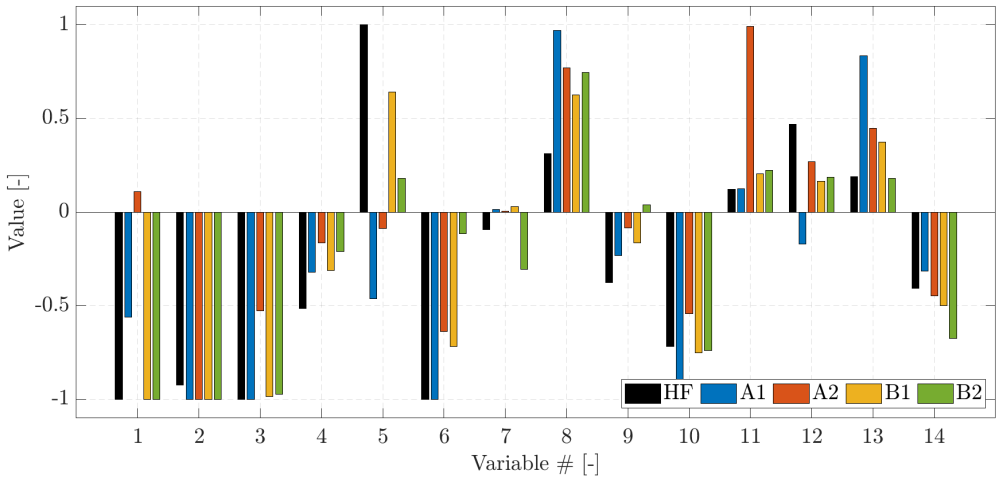

Fig. 5 Variable values of the optimized hulls.

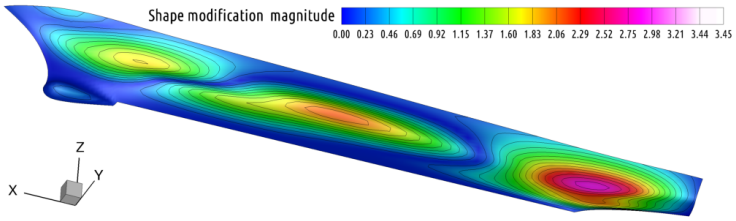

(a) HF

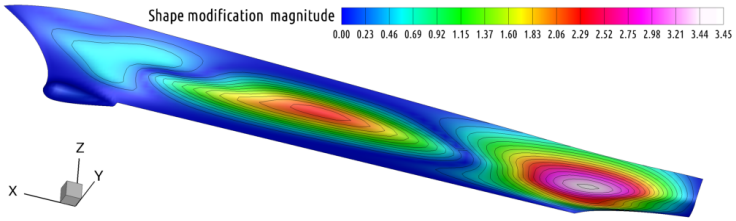

(b) MF (A1)

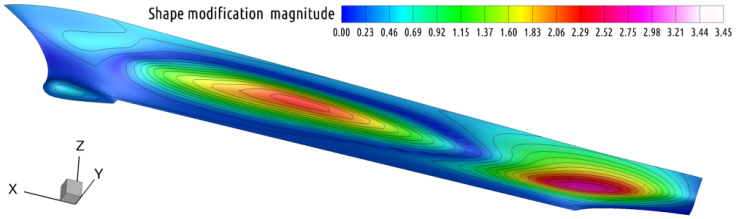

(c) MF (A2)

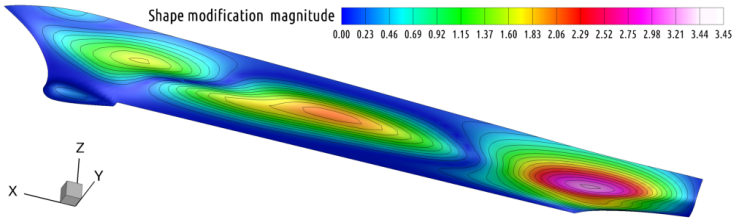

(d) MF (B1)

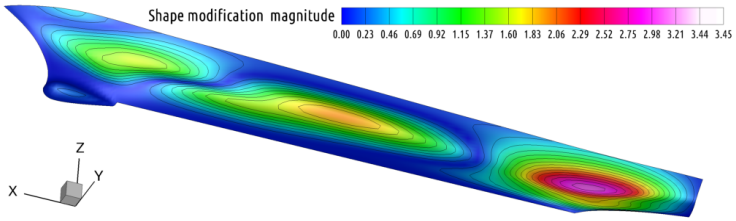

(e) MF (B2)

Fig. 6 Shape modification magnitude of the optimized hulls with respect to the original hull.

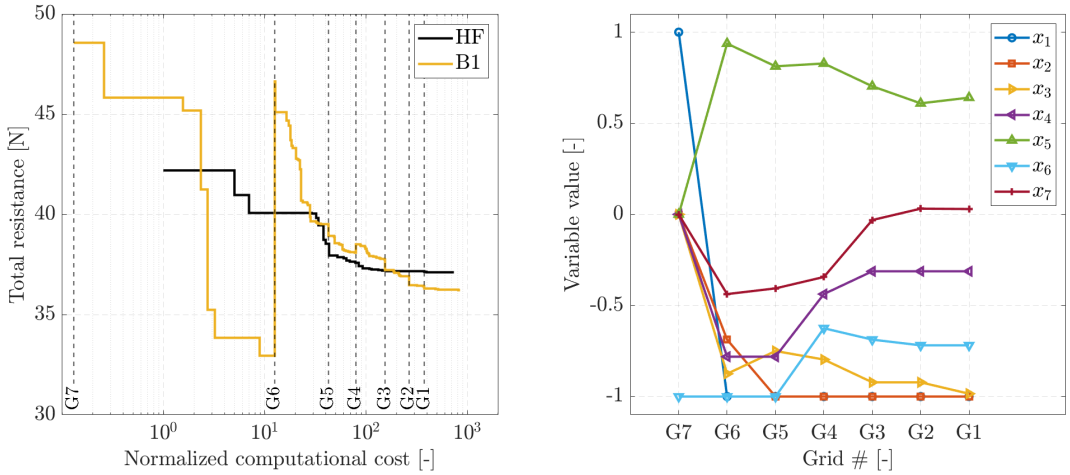

(a) Convergence of the total resistance.

(b) Convergence of the first six variables.

Fig. 7 Convergence of the B1 setup.

Figure 4 shows the comparison between the HF and MF optimizations. The convergence is reported versus the normalized computational cost. MF optimizations start with a lower initial computational cost since the first evaluation is performed on the coarsest grid G7. The convergence of the MF optimizations shows significant changes in the objective function value when the algorithm switches among the coarser grids. Except A2, all the MF optimizations achieve better optima solutions (lower total resistance) than the high-fidelity optimization. Furthermore, the MF optimizations achieve a lower value of the total resistance with a reduced computational cost then the high-fidelity optimization. The use of a dynamic threshold (B setups) produces better results than using a fixed threshold for all grids (A setups). The algorithm's performance seems to be more affected by the threshold value than by the steplength reinitialization.

Figure 5 shows the optimized variables values. Except A2, all the optimizations show similar variable values for

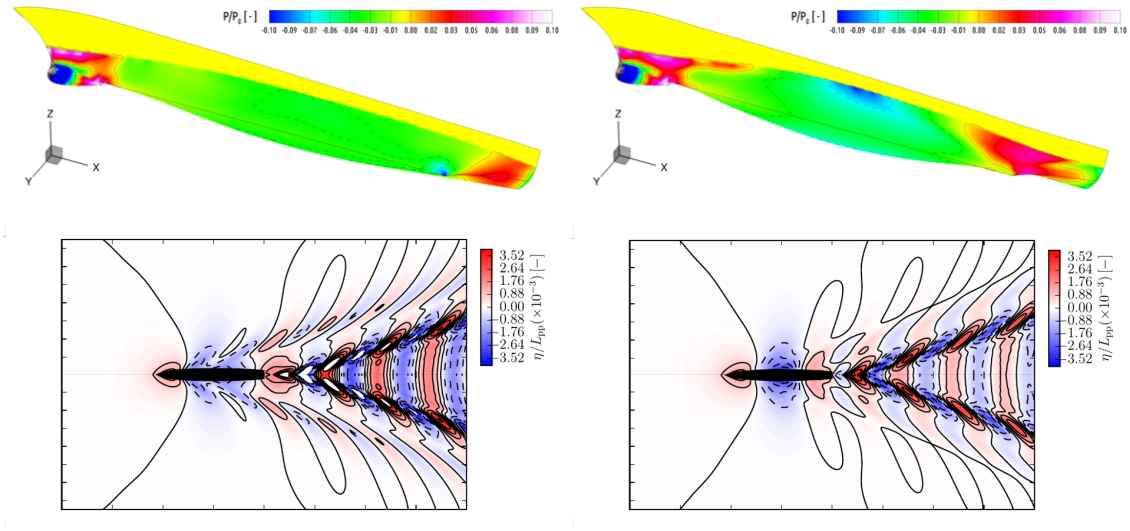

Fig. 8 Pressure on hull (top) and free-surface elevation (right) of the original model hull (left) compared to the B1 optimum (right).

Table 4 B1 setup, percentage total resistance variation when switching grid.

Switching	Resistance variation [%]
G7 → G6	45.5
G6 → G5	-1.5
G5 → G4	1.0
G4 → G3	-1.4
G3 → G2	-1.2
G2 → G1	-0.3

x_1, x_2, x_3, x_4. Greater differences are present when comparing the other variables. Since the first variables are those that have a more significant effect on the shape modification than the others, it is possible to state that all the MF optimizations achieve similar hull-shapes. Figure 6 shows the hull-shape modification magnitude of the optimized hulls with respect to the original hull. Setups A focus the hull-shape modification in the mid-length and aft regions (bi-modal), whereas B setups distribute the modification between the bow, mid-length, and aft regions (tri-modal). A2 performs a greater modification of the sonar dome and a smaller modification of the aft region, in comparison with the other optimizations. Overall, the shape modifications provided by the different setups are similar, with localized differences.

Figure 7 shows the convergence and the value of the first six variables for the B1 setup. Figure 7a shows that switching from G7 to G6, the resistance value changes abruptly achieving a value slightly lower than the starting point. Similarly, when switching from G5 to G4 the resistance is increased, but to a lower value than the initial resistance value on G5. This means that the algorithm is exploiting the region of the minimum. On finer grids, the resistance decrease is smaller, meaning that the algorithm is close to convergence. It is worth noting that when the algorithm starts evaluating the objective function on G1, the starting point (convergence point of G2) already shows a resistance value lower than the final resistance value of the high-fidelity optimization. Figure 7b shows that the variables value significantly changes when switching from G7 to G6 and from G5 to G4. x_1 and x_2 converge already with G5, whereas the values of x_3 and x_5 changes for all the grids.

Table 4 summarizes the variation of the evaluated resistance as percentage with respect to the value on the previous converged grid. It is worth noting that the switch from the coarsest grid produces a significant increase of the evaluated resistance. This means that the G7 grid did not lead the algorithm in a region that is close to the minimum. Differently, the switch towards the other grids lead to a decrease of the evaluate resistance, except between G5 and G4. This means that the grid G7 is too coarse and the response function it can provide is not well correlated with the response as computed on the finer grids.

Figure 8 shows a comparison between the original and the optimized hull according to B1 setup. The optimized shows a more prominent cavity in the front and rear regions of the hull resulting in a lower wave elevation behind the hull.

V. Conclusions and Future Work

An extension is proposed of the linesearch-based derivative-free approach for nonsmooth constrained optimization for multi-fidelity optimization, where the objective function evaluation is performed with variable accuracy. The proposed algorithm starts exploring the coordinate directions, evaluating the objective function at the lowest accuracy. Then, when the convergence defined by a steplength value is achieved, the accuracy of the evaluation of the objective function is increased and the steplength is reinitialized. The process is repeated until the algorithm convergences while using the highest accuracy. The algorithm has been applied to the hull-shape optimization of the DTMB 5415 model, an open-to-public model of a naval destroyer. The hull-shape modifications are provided by $N = 14$ design variables, defined by a physics-informed dimensionality reduction procedure. Multi-fidelity is achieved defining seven discretizations of the computational domain. For each grid an error associated to the objective function evaluation has been defined. Four algorithm's setups have been tested. Specifically, a static and a dynamic convergence value of the steplength are considered. The dynamic threshold is set equal to the grid error value. For each threshold, a static and a dynamic reinitialization value of the steplength parameter are considered. The dynamic reinitialization is based on the steplength convergence value on the last converged grid. The four setups have been compared with the algorithm

performing an optimization using only the highest-fidelity available.

Three out of four setups have performed better than the high-fidelity optimization. The multi-fidelity optimizations converge to a lower resistance value and with a lower computational cost than the high-fidelity optimization. Therefore, the multi-fidelity method is more efficient in identifying the minimum region and provides better exploitation of the design space. The use of a dynamic threshold value for the steplength parameter (B setups) produces better results than the same fixed threshold for all grids (A setups).

The use of a dynamic threshold equal to the grid error produces better results than a static threshold because the algorithm spends less time on the coarser grids, where the region of the minimum is likely less correlated with the higher fidelities. Therefore, the definition of the different grids should be done taking into account their correlation, in order to provide the convergence of the algorithm towards the region of the minimum also when the objective function is evaluated on the coarsest grid. Finally, the algorithm's performance seems to be more affected by the threshold value than by the steplength reinitialization.

Future work focuses on including the hull dynamic trim and sinkage, therefore using the coupling between the hydrodynamics and the rigid body equation of motions. This physical coupling introduces an additional fidelity level. Finally, mixed integer optimization will be used, to include the number of variables defined by the physics-informed dimensionality reduction as a design variable.

Acknowledgments

CNR-INM is grateful to Dr. Woei-Min Lin, Dr. Elena McCarthy, and Dr. Salahuddin Ahmed of the Office of Naval Research and Office of Naval Research Global, for their support through NICOP grant N62909-18-1-2033. Dr. Riccardo Pellegrini is partially supported through CNR-INM project OPTIMAE. The work is conducted within the NATO AVT-331 task group on "Goal-driven, multi-fidelity approaches for military vehicle system-level design".

References

[1] Beran, P. S., Bryson, D. E., Thelen, A. S., Diez, M., and Serani, A., "Comparison of Multi-Fidelity Approaches for Military Vehicle Design," *21th AIAA/ISSMO Multidisciplinary Analysis and Optimization Conference (MA&O), AVIATION 2020*, Virtual Event, June 15-19, 2020.

[2] Baar, J. d., Roberts, S., Dwight, R., and Mallol, B., "Uncertainty quantification for a sailing yacht hull, using multi-fidelity kriging," *Computers & Fluids*, Vol. 123, 2015, pp. 185 – 201.

[3] Serani, A., Pellegrini, R., Wackers, J., Jeanson, C.-E., Queutey, P., Visonneau, M., and Diez, M., "Adaptive multi-fidelity sampling for CFD-based optimisation via radial basis function metamodels," *International Journal of Computational Fluid Dynamics*, Vol. 33, No. 6-7, 2019, pp. 237–255.

[4] Rumpfkeil, M. P., and Beran, P. S., "Multi-Fidelity, Gradient-enhanced, and Locally Optimized Sparse Polynomial Chaos and Kriging Surrogate Models Applied to Benchmark Problems," *AIAA Scitech 2020 Forum*, 2020, p. 0677.

[5] Coppedè, A., Gaggero, S., Vernengo, G., and Villa, D., "Hydrodynamic shape optimization by high fidelity CFD solver and Gaussian process based response surface method," *Applied Ocean Research*, Vol. 90, 2019, p. 101841.

[6] Yi, J., Shen, Y., and Shoemaker, C. A., "A multi-fidelity RBF surrogate-based optimization framework for computationally expensive multi-modal problems with application to capacity planning of manufacturing systems," *Structural and Multidisciplinary Optimization*, 2020, pp. 1–21.

[7] Fasano, G., Liuzzi, G., Lucidi, S., and Rinaldi, F., "A linesearch-based derivative-free approach for nonsmooth constrained optimization," *SIAM Journal on Optimization*, Vol. 24, No. 3, 2014, pp. 959–992.

[8] Bassanini, P., Bulgarelli, U., Campana, E. F., and Lalli, F., "The wave resistance problem in a boundary integral formulation," *Surveys on Mathematics for Industry*, Vol. 4, 1994, pp. 151–194.

[9] Lucidi, S., and Sciandrone, M., "A Derivative-Free Algorithm for Bound Constrained Optimization," *Computational Optimization and Applications*, Vol. 21, No. 2, 2002, pp. 119–142.

[10] Liuzzi, G., Lucidi, S., and Rinaldi, F., "Derivative-free methods for bound constrained mixed-integer optimization," *Computational Optimization and Applications*, Vol. 53, 2012, pp. 505–526.

[11] Diez, M., Serani, A., Campana, E. F., Goren, O., Sarioz, K., Danisman, D. B., Grigoropoulos, G., Aloniati, E., Visonneau, M., Queutey, P., and Stern, F., "Multi-objective Hydrodynamic Optimization of the DTMB 5415 for Resistance and Seakeeping," *Proceedings of the 13th International Conference on Fast Sea Transportation, FAST 2015*, Washington, D.C., USA, 2015.

[12] Serani, A., Campana, E. F., Diez, M., and Stern, F., "Towards Augmented Design-Space Exploration via Combined Geometry and Physics Based Karhunen-Loève Expansion," *18th AIAA/ISSMO Multidisciplinary Analysis and Optimization Conference (MA&O), AVIATION 2017*, Denver, USA, June 5-9, 2017.

[13] Serani, A., Diez, M., Wackers, J., Visonneau, M., and Stern, F., "Stochastic shape optimization via design-space augmented dimensionality reduction and rans computations," *57th AIAA Aerospace Sciences Meeting, SciTech 2019*, 2019, p. 2218.